One Good Turn

Farhood Azarsina

Dr. Neil Bose

Dr. Mohammad Saeed Seif

Azarsina, Bose and Seif describe a numerical simulation of an underwater vehicle maneuvering under the action of its dynamic control systems in deep calm water.

Who should read this paper?

AUV designers and operators with an interest in dynamic control systems and vehicle maneuvrability are likely to find the variation in simulated manoeuvering behaviour with vehicle geometry changes of interest.

Why is it important?

The paper shows the effect of rudder angle and vehicle geometry on the vehicle turning maneuver. The results apply to a wide range of torpedo-shaped underwater vehicle hulls.

The accuracy of the simulation results is comparable to the real maneuvering of an underwater vehicle if the coefficients are accurate for a given vehicle, but the cost involved is obviously much less.

A modified version of the simulation code developed during this research might be incorporated into maneuvring simulators for operator training.

For vehicle navigation and tracking this simulation accounts for the dynamics of the dynamic control loop.

About the authors

Farhood Azarsina holds a Bachelor and Master of Science in Mechanical-Marine Engineering from Sharif University of Technology and is currently a Doctoral student in Ocean Engineering and Naval Architecture at Memorial University of Newfoundland. His particular areas of expertise are underwater vehicle dynamics and control, and marine hydrodynamics.

Dr. Neil Bose is a Professor and Canada Research Chair in Offshore and Underwater Vehicles Design at Memorial University. His areas of expertise are underwater vehicles and marine propulsion.

Dr. Mohammad Saeed Seif is an Associate Professor and Marine Engineering Laboratory Head at Sharif University of Technology. His areas of expertise are marine hydrodynamics, offshore engineering and numerical fluid dynamics.

AN UNDERWATER VEHICLE MANEUVERING SIMULATION; FOCUS ON TURNING MANEUVERS

Farhood Azarsina[1], Neil Bose[2], Mohammad S. Seif[3]

[1] *PhD Student, Faculty of Engineering & Applied Science, Memorial University*
[2] *Professor, Faculty of Engineering & Applied Science, Memorial University*
[3] *Associate Professor, Department of Mechanical Engineering, Sharif University of Technology*

e-mail: Farhood.Azarsina@nrc.ca

ABSTRACT

Maneuvering of an underwater vehicle was studied under the action of its dynamic control systems. The equations of motion were solved numerically in the original state without any linearization or other simplification. The underwater vehicle was assumed to be a rigid body with 6 DOF (Degrees Of Freedom) moving in calm water. To reduce the complexity of the real motion, some simplifying assumptions were applied to the hydrodynamic forces and moments. The computer code developed, using MATLAB™7.1, can simulate versatile states of the underwater vehicle maneuvering. As an example, the turning maneuvers are demonstrated in detail. The simulation is applicable to either large manned submarines or AUVs (Autonomous Underwater Vehicles), however the sample simulations are performed for large submarines.

Key words: Dynamics of an underwater vehicle, numerical simulation, maneuvering

1. INTRODUCTION

This paper focuses on dynamic control systems and their effect on the maneuvering of an underwater vehicle. The dynamic control systems are effective in 6 DOF and use lift and propulsion forces to navigate the underwater vehicle. Generally an underwater vehicle has two kinds of maneuvering control systems:

1. The systems that can act in the stationary state, named: Static
2. The systems that are activated when there is a relative velocity between the vehicle and water, named: Dynamic.

In Figure 1 the degrees of freedom under the control of each of these systems are shown. As can be seen in Figure 1, the static control systems are effective in three DOF [Allmendinger 1990].

An underwater vehicle should have a stable dynamic behavior such that without changing its control surfaces or propelling force, it should keep its path in calm water. On the other hand, the underwater vehicle, if necessary, must be able to change its path and speed yet safely and quickly attain stability. Usually in addition to dynamic stability, details of response such as: overshoot, rise time and peak time are important so as the vehicle can fulfill the mission requirements.

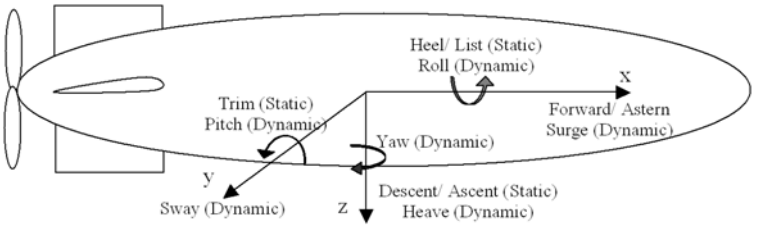

Figure 1. Degrees of freedom and the corresponding control systems.

Conventionally, dynamic control systems include propeller(s), thrusters, and control surfaces. The control surfaces of an underwater vehicle are rudders, stabilizers, and bow and stern hydroplanes. Application of the dynamic control systems depends on the velocity. Low speed maneuvering is very important for underwater vehicles. Many missions of an underwater vehicle require an almost constant position to be held for a measurement to be taken. The propeller has an important role in the low speed maneuvering. For optimum performance, the propeller should have a large diameter and rotate slowly. Modern trends of underwater vehicle design have gone toward streamlined, teardrop body shapes and longer and simpler deep-water mission possibilities have resulted in the popularity of large-diameter single propeller design. ROV type vehicles are another solution, but the tether limits the types of mission profiles possible.

The thrusters, if they are effectively designed and installed in the correct place, can assist maneuvering at both low and high speed. Using thrusters is mostly beneficial in ROVs (Remotely Operated Vehicles), which need many controlled degrees of freedom and which may have no control surfaces. But for the manned submarines and streamlined AUVs, thrusters significantly interrupt the hydrodynamic shape of the bare hull and are not usually used; though there are exceptions such as the AUV, Autonomous Benthic Explorer (ABE).

The control surfaces have airfoil sections. The drag force exerted on these surfaces does not assist maneuvering. The lift is proportional to the square of the speed, thus the control surfaces are not very useful at low speed. On the other hand, the lift force is proportional to the planform area of the control surface. Hence, the larger the span for a given chord, the greater the lift force. Large span, also, means that the surface operates outside of the boundary layer of the underwater vehicle hull. However, it increases the risk of collision and makes the navigation cumbersome. As mentioned, rudders, stabilizers and bow and stern hydroplanes are the main control surfaces of an underwater vehicle. Stern hydroplanes conduct the underwater vehicle motion in the x-z plane. Bow hydroplanes are the most effective tools to maintain and preserve a constant depth near the water surface (periscope depth). More information on underwater vehicle systems can be found in Allmendinger [1990], Burcher and Rydill [1995], Griffiths [2003] and SUBTECH'87-Vol.14 [1988].

In this research, utilizing the aforementioned concepts, an underwater vehicle was modeled and its motion was simulated numerically. The logical consistency of the response and convergence of the response with respect to the time step of the numerical analysis was observed. Turning maneuver data from a free-running model test was used to validate the simulation and then the turning maneuvers as a sample of the capabilities of the code were discussed in detail. Some of the most important restrictions of the developed software are listed in the next section. The future plan is to upgrade the code using experimental data and validate it using data from free-running maneuvers.

2. EQUATIONS OF MOTION AND BASIC ASSUMPTIONS

According to the mathematical model introduced and explained by Fossen [1994] and Azarsina [2004], the Newton-Euler equation of motion for an underwater vehicle is

$$M_{RB}\dot{v} + C_{RB(v)}v = \tau_{RB} \tag{1}$$

In equation (1), M_{RB} is the 6×6 mass matrix of the underwater vehicle and C_{RB} is its added inertia. In fact, C_{RB} includes vectors of Coriolis effect, $v_2 \times v_2$, and centrifugal effect, $v_2 \times (v_2 \times r_G)$ where v is the underwater vehicle's linear and angular velocity vector and is defined as

$$v = [v_1, v_2];\ v_1 = [u, v, w];\ v_2 = [p, q, r] \tag{2}$$

$\dot{v}$ is the underwater vehicle acceleration vector. In equation (1), τ_{RB} is the 6×1 vector of forces and moments exerted on the underwater vehicle and can be written as

$$\tau_{RB} = \underbrace{\tau}_{\substack{\text{propulsion}\\ \text{forces}}} - \underbrace{M_A\dot{v} - C_{A(v)}v}_{\substack{\text{hydrodynamic}\\ \text{added mass}}} - \underbrace{D(v)}_{\substack{\text{hydrodynamic}\\ \text{damping and lift}}} + \underbrace{g(\eta)}_{\substack{\text{restoring}\\ \text{forces}}} \tag{3}$$

The equation of motion, (1), is written in the local vehicle coordinate system. Consequently, the hydrodynamic forces and moments do not depend on the vehicle orientation in the global coordinate system. In equation (3), M_A is the added mass and C_A is the added inertia of the added mass. The same definition is used here; that C_A is the inertia due to the Coriolis and centrifugal accelerations. The resultant hydrodynamic drag and lift force and moment is denoted by *D*. It is better to decompose the hydrodynamic forces into two parts: the forces exerted on the bare hull and the forces exerted on the control surfaces and other appendages.

The 6×1 vector τ is the propulsion force and moment vector. The 6×1 vector $g(\eta)$ is the resultant vector of buoyancy and gravity forces, which is a function of the position and heading vector and therefore is originally derived in the global coordinate system. It can be transformed into the local coordinate system by matrix transformation. Details of the above parameters and algorithms of the modeling are presented by Azarsina and Seif [2005]. In addition to these forces, contact forces should be considered in a complete analysis as well.

External moving or stationary bodies, waves and underwater currents are the sources of contact forces. In general, the major assumptions in this study are as follows:

- The water is assumed to be calm; the waves and underwater currents are not modeled.
- The vehicle is assumed to be a rigid body; therefore the effects of internal moving masses, including ballast water with a free surface, are not modeled.
- In the mass matrix calculation, mass and inertia of the hull are assumed to be dominant and the mass and inertia of the appendages are ignored. In addition, the underwater vehicle is assumed to be neutrally buoyant with zero trim angle.
- The hydrodynamic added mass coefficients are obtained by the theoretical formulae for slender bodies with smooth sections. Added mass of the appendages is ignored.
- The hydrodynamic damping and lift forces are calculated separately for the hull and appendages. But, the interaction effect between the hull and appendages is not included.
- Experimental results for the limited range of [-25, 25]° AOA (angle of attack) are used to estimate drag and lift coefficients of the bare-hull. For larger AOA,

constant coefficients are assumed and the forces and moments are assumed to depend only on the projected area. The results shown here are all maneuvers with small angles of attack, therefore we are always within the [-25, 25]° range.

- The same procedure applies to the drag and lift of the control surfaces for large AOAs.
- For the high-rate maneuvers, as in obstacle avoidance, the coefficients depend on the rate of the turn. In this modeling, the coefficients only depend on the angles, not their rate of change.

Using this approach it is felt that the dominant phenomena in the maneuvering of an underwater vehicle, as is illustrated in the results section, have been modeled; that is, the major forces and moments are included and no linearization is applied to the equations of motion. For further studies, equations (1) and (3) as the basic approach can be kept then each term can be investigated in more detail.

3. MODELING

(a) Model geometry

Suggested by Froude in 1877 [Jackson 1983], the bare hull of an underwater vehicle can be defined by three distinguished parts: after body, parallel-sided mid-body, and fore body. Our underwater vehicle geometry is defined according to the form suggested by Froude with Nystrom equations and coefficients as in equation (4). The model dimensions are modifiable as inputs of the software; therefore the mentioned geometry covers most of the conventional as well as modern underwater vehicles. The radius of the bow (fore) and stern (aft) circular cross-sections are given by equation (4), proposed by Nystrom in 1868 and referred to by Jackson [1983]

$$y_f = \frac{d}{2}\left[1-(x_f / l_f)^{n_f}\right]^{1/n_f}, \qquad y_a = \frac{d}{2}\left[1-(x_a / l_a)^{n_a}\right] \tag{4}$$

Indices a and f represent aft and fore ends of the underwater vehicle, respectively, d is the maximum diameter, l the overall length of each part, and x the distance from maximum diameter section. In equation (4), $n_f = 2.25$ and $n_a = 2.75$. The complete form of the bare hull, given by Froude, includes a parallel-sided mid-body between the fore and aft end. The underwater vehicle rigid body density is assumed to be uniform in all directions and the hull is symmetric with respect to the x-axis, therefore the center of gravity is on the x-axis. To maintain a constant depth in the initial state, two conditions are required.

$$W = B \quad \text{and} \quad r_G = r_B \tag{5}$$

where W and B are weight and submerged buoyancy of the vehicle, and r_G and r_B are the position vectors of center of gravity and center of buoyancy in the local coordinate. To simplify the moment of inertia calculations, the origin of the local coordinate system is assumed to be coincident with the center of gravity and consequently the center of buoyancy, i.e.

$$r_G = r_B = [0,0,0] \tag{6}$$

Note that the position of COB is calculated while the geometry of the model is being defined, and then the local coordinate's origin and COG are defined to be coincident with COB. The developed computer code uses an average value extracted from the statistical curves from [Jackson

1983] to assign a displacement, m, to a length-to-diameter ratio, l/d, for a special length or diameter, both of which should have been defined previously by the user. The curves are based on data from manned submarines, but the data can be scaled for AUVs. Having the total mass (displacement), the total volume is known. Note that no free-flooded volume is included in the model. Thus, the first steps of the modeling can be summarized as follows: the user defines l and d, the underwater vehicle mass is interpolated and determined from the statistical curves, total volume then is known, this volume is constituted of fore, parallel body, and aft volumes

$$\nabla = \nabla_f + \nabla_p + \nabla_a \tag{7}$$

For the parallel body the index p is used. Then the general shape of the underwater vehicle can be obtained and drawn using equations (4) to (7). The general shape is a function of the length of fore, aft, and parallel body. For instance, if the length and diameter of the underwater vehicle are $l = 70$ m and $d = 12$ m, then, assuming that the fore body has one-fifth of the overall length, the characteristics shown in Table 1 result. The one-fifth value for the fore body is selected according to the experimental observations of Loid and Bystrom [1983]. Distance of the COB from the vehicle's fore end is x_B. The form of the underwater vehicle bow is shown in Figure 2. Note that the x-axis in Figure 2 shows the distance from the local coordinate origin, which is COB, but x_f in equation (4) is zero at the left end of Figure 2. Graphical layouts of the stern and parallel body are obtained in the same manner. Having the geometry, the restoring force (gravitational and buoyancy force) is easily derived. Here, according to equation (5) the net restoring force is zero.

l_f	l_a	l_p	x_B (distance from fore end)	m
14 (m)	45.27 (m)	10.73 (m)	29.15 (m)	5.52E+06 (kg)

Table 1. Model characteristics for $l = 70$ m and $d = 12$ m.

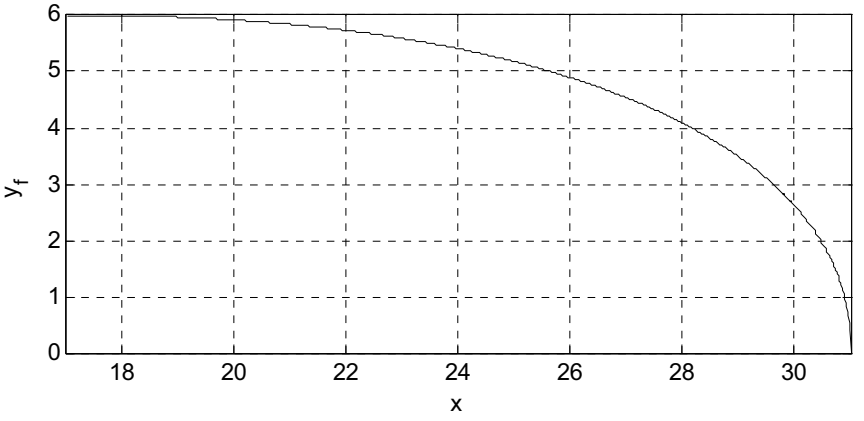

Figure 2. Bow shape of the underwater vehicle of $l/d = 70/12$.

(b) Bare Hull Hydrodynamic Forces

(i) *Drag and lift*

As mentioned, to determine the hydrodynamic forces and moments, it is better to study the bare hull and appendages separately. For the bare hull, for small angles of attack using the Taylor expansion, ignoring the higher order terms, one can write

$$\cos\alpha \cong 1-\frac{\alpha^2}{2}, \quad \sin\alpha \cong \alpha \tag{8}$$

and then the drag force on the bare hull is [Ridley 2003]

$$\begin{aligned} D_x &= \frac{1}{2}\rho A_f C_{D(\beta)} u^2 (1+\beta^2)(1-\frac{\beta^2}{2}) \\ D_y &= \frac{1}{2}\rho A_f C_{D(\beta)} u^2 (1+\beta^2)\beta \\ D_z &= \frac{1}{2}\rho A_f C_{D(\gamma)} u^2 (1+\gamma^2)\gamma \\ \beta &= \frac{v}{u} \quad , \quad \gamma = \frac{w}{u} \end{aligned} \tag{9}$$

The drag coefficient for the bare hull fitted to the experimental data from a small underwater vehicle is shown in Figure 3 [Ridley 2003]. The quadratic fit, which does not match the experimental data very well but goes through an average of them, is

$$1000 * C_{D(\alpha)} = 1.317\alpha^2 + 724.5 \tag{10}$$

Note that the bare hull is a body of revolution and its dependence on the AOA is the same for β or γ, hence denoted in general by α in equation (10). The lift forces and turning moments due to the drag and lift forces on the bare hull are derived in the same way.

(ii) Added mass

The bare-hull is a body of revolution and according to equation (6) COG and COB coincide, thus according to Humphreys [1978] and Jones [2002] the cross terms in the added mass matrix can be ignored, meaning that the added mass will be a diagonal matrix:

$$M_A = diag\{X_{\dot{u}}, Y_{\dot{v}}, Z_{\dot{w}}, K_{\dot{p}}, M_{\dot{q}}, N_{\dot{r}}\} \tag{11}$$

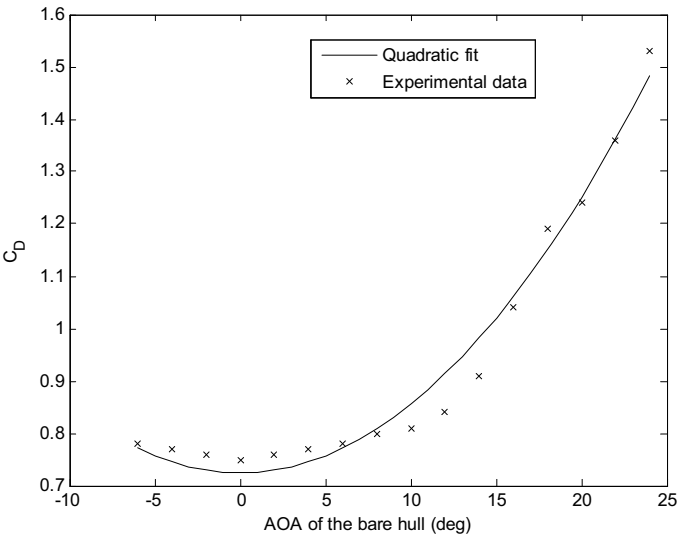

Figure 3. Drag coefficient for the bare hull [Ridley 2003].

The elements of this diagonal matrix, for three-dimensional completely submerged slender bodies, are approximated theoretically (strip theory) as follows

$$
\begin{aligned}
X_{\dot{u}} &= \int_{-l/2}^{l/2} A_{11}^{2D}(y,z)\,dx \approx 0.1m \\
Y_{\dot{v}} &= \int_{-l/2}^{l/2} A_{22}^{2D}(y,z)\,dx \\
Z_{\dot{w}} &= \int_{-l/2}^{l/2} A_{33}^{2D}(y,z)\,dx \\
K_{\dot{p}} &= \int_{-l/2}^{l/2} A_{44}^{2D}(y,z)\,dx \\
M_{\dot{q}} &= \int_{-l/2}^{l/2} A_{55}^{2D}(y,z)\,dx \\
N_{\dot{r}} &= \int_{-l/2}^{l/2} A_{66}^{2D}(y,z)\,dx
\end{aligned}
\qquad (12)
$$

All the elements of the diagonal added mass matrix in equation (11) are defined in equation (12) as the integral of the fluid mass displaced by the 2D differential cross-sections $A_{ii(y,z)}^{2D}$. For the first term, $X_{\dot{u}}$, the result is approximately one-tenth of the total mass of the submerged body, which is almost the same value as the Lamb's coefficient for the 2D ellipsoid in potential flow [Humphreys 1978]. The integrand $A_{ii(y,z)}^{2D}$ is the mass of the fluid displaced with a 2D cross section in the *y-z* plane, perpendicular to the longitudinal axis of the slender body. The length of the section is dx. The magnitude of for A_{22}, A_{33}, A_{44} some special cross sections are derived experimentally [Fossen 1994] and A_{55}, the pitching moment due to added mass effect or pitch added inertia, is the sum of the moment of heave and surge added mass around the corresponding axes. Sway and surge added mass terms contribute in the yaw added inertia, A_{66}.

(c) Control surfaces

The next step is to model control surfaces. It is assumed that the model has two stern hydroplanes (horizontal) and two rudders (vertical). In the following expressions and equations, hydroplanes are denoted by index *p* and rudders are denoted by *r.* A typical hydrofoil here is assumed, that is, the coefficients C_D, C_L, C_M for the control surfaces neither are obtained by theory nor correspond to a tested profile. However, the data are in the range of real data of the standard profiles (e.g. NACA, Eppler, etc.). Figure 4 shows these typical drag, lift, and moment coefficients.

All four surfaces are identical, namely the same geometry and the same coefficients. In a real design due to the differences in application, the hydroplanes and rudders might have different designs. Having C_M, C_L, C_D versus the angle of attack, the forces and moments of each control surface can be evaluated as a function of the attack angle. Also, the stall angle is assumed to be 20°, after which the coefficients are assumed to be constant.

The angle of attack of the control surface relative to water is equal to the sum of the user defined angle and the angle of attack of the hull relative to water, i.e.

$$a_p = a_{p0} + \gamma' \qquad (13)$$

where a_{p0} is the initial angle of the hydroplane relative to the underwater vehicle hull defined by the user, and the AOA of the hull at the position of the hydroplanes relative to water is defined as

$$\gamma' = \frac{w + x_p q}{u} \qquad (14)$$

In fact the above ratio is $\tan\gamma'$, and since the angle γ' is small, its value can be assumed equal to its tangent. It is

assumed that the surge velocity is much greater than sway and heave velocity in deep-water maneuvering. x_p is the distance of the center of pressure of the hydroplanes from the local coordinate origin. The term $x_p q$ appears as a result of the underwater vehicle pitch velocity at the location of the stern hydroplanes. By the same concept, for the rudders we have

$$a_r = a_{r0} + \beta' \tag{15}$$

$$\beta' = \frac{v - x_r r}{u} \tag{16}$$

The terms have the same definition but for the rudder with index *r*, and the corresponding directions. The term $x_r r$ appears as a result of the underwater vehicle's yaw velocity at the location of therudders. To interpret the minus sign, note the positive direction of *r* and *v* velocities in Figure 1.

The stern hydroplanes generate a turning moment about the y-axis and the rudders generate a turning moment about the z-axis, both of which can be evaluated by a simple vector product of the lift force and the turning moment arm. The turning moment arm is x_p or x_r. Moreover, both stern hydroplanes and rudders generate a moment about the x-axis. The turning arm in this direction is assumed to be half of the span of each control surface. When the port and starboard hydroplanes and up and down rudders have the same angle of attack, the turning moment about x-axis due to control surfaces is expected to be zero. Then the 6×1 vector of force and moment due to the control surfaces is determined.

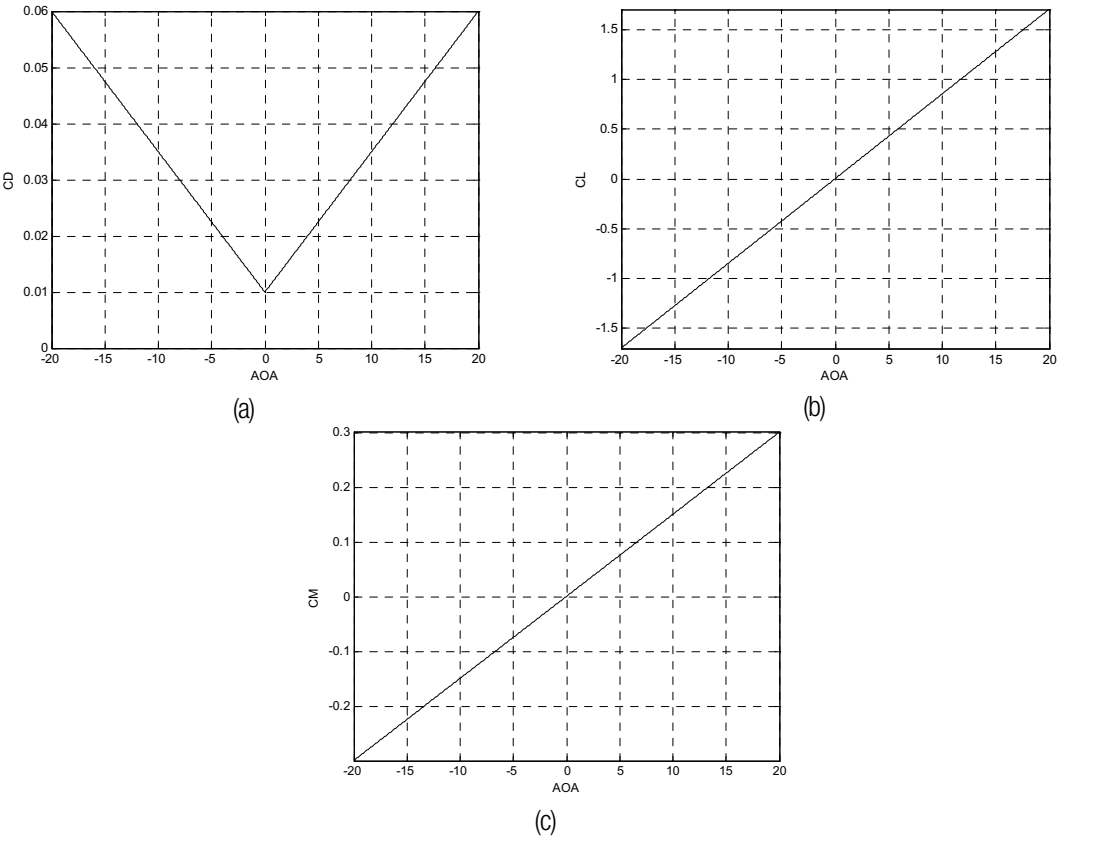

Figure 4. Typical (a) drag, (b) lift, and (c) moment coefficients for the control surfaces.

(d) Propeller

Next, the propulsion is modeled. It is supposed that the model has one propeller at the aft end and no thrusters, which is the trend of modern underwater vehicle design, thus the propulsion force is

$$\tau = [\rho\, d_p^4\, K_T\, J\, n^2, 0, 0,\ \rho\, d_p^5\, K_Q\, J\, n^2, 0, 0] \quad (17)$$

In the above matrix, d_p is the propeller diameter, K_T and K_Q are the thrust and torque coefficients and the propeller advance coefficient is defined as

$$J = V_a / (n.d)_p \quad (18)$$

Water velocity through the propeller disc is

$$V_a = (1-\omega)\, U \quad (19)$$

The forward speed of the vehicle is U and the Taylor wake coefficient, ω, is estimated with the empirical formulae resulting from model tests, see [Allmendinger 1990]. Diagrams of propeller coefficients K_T, K_Q, η versus the advance ratio J for various series of fixed-pitch propellers are available in Carlton [1994] or Kuiper [1992]. A typical propeller was selected to quantify the parameters for the software. The user defines the propeller diameter and its rpm. The speed of rotation of the propeller, n, in all the formulae should be converted to rad/s. In this modeling a main propeller is assumed that is composed of two three-bladed propellers in series installed on one shaft, with opposite blade pitch, so as to reduce or ideally diminish the propeller torque, therefore the propulsion vector in equation (17) is only the surge force.

(e) Numerical Solution

From equations (1) and (3) the equation of motion is in the form

$$\tau - M_A \dot{v} - C_{A(v)} v - D(v) + g(\eta) = M_{RB} \dot{v} + C_{RB(v)} v \quad (20)$$

which by algebra simplifies into

$$(M_{RB} + M_A)\dot{v}_{(t_0)} = C_{(t_0)} \quad (21)$$

The RHS of equation (21), $C_{(t_o)}$, is calculated at the start of the motion by substituting the initial velocity and position in the terms that depend on the velocity and position vectors in equation (20). Also it is convenient to write

$$M = M_{RB} + M_A \quad (22)$$

Therefore, the underwater vehicle's acceleration at the instant t_0 is

$$\dot{v}_{(t_0)} = M^{-1} C_{(t_0)} \quad (23)$$

Integration of the acceleration in the time interval (δt) gives velocity at the instant ($t_0 = \delta t$), and then gives position results from the velocity transferred to the global coordinate system and integrated.

4. RESULTS AND DISCUSSION

Comparison of the simulation results for different integration time steps was employed to verify the convergence of the code. Then the simulation result was compared to a free-running model test to validate the code. However, due to simplifying assumptions in the geometric and hydrodynamic modeling of the vehicle, the

magnitude of response is not expected to accurately simulate the real maneuvers in a quantitative manner. Unless explicitly mentioned, in all the simulations the vehicle is at the initial position of $[0,0,z_0]$ that is at an initial z_0 depth, and its orientation, $[\varphi,\theta,\psi]$, is initially [0,0,0]. All the initial velocities are zero, but to initiate the motion, according to equations (17) to (19), a very small initial surge velocity (0.01 m/s) is defined. Except in section 4(b) the models are large submarines of length of some ten meters. In section 4(b) the dimensions are of the same order of magnitude as the US Coast Guard 47ft motor lifeboat.

(a) Simulation Convergence

Table 2 shows the initial conditions of the dynamic control systems for a vehicle with l=70 m and $d=12$ m, for which the basic characteristics are shown in Table 1. The leading edge of the control surfaces is assumed to be $0.92\times l$ away from the fore end of the vehicle and their center of pressure is one-fourth of their chord-length back from their leading edge. Then, knowing the position of the center of buoyancy gives the moment arm of the control surfaces, x_p and x_r.

For such a case, that is, an initially stationary vehicle with zero rudder angle and constant propeller speed of 150 rpm, Figures 5, 6 and 7, respectively, show the diagrams of position, velocity and acceleration of the underwater vehicle in the surge direction over 160 seconds. The motion has been simulated with four different time steps of 0.05, 0.5, 2 and 4 seconds. Note that in all of the following figures, position is stated in the global or earth-fixed coordinates, but velocity and acceleration (force) are stated in the local or body-fixed coordinates.

a_{p0} (deg)	a_{r0} (deg)	x_p, x_r (m)	d_p (m)	n (rpm)
0	0	32.25	5.4	150

Table 2. Initial conditions of the dynamic control systems for $l=70$ m and $d=12$ m.

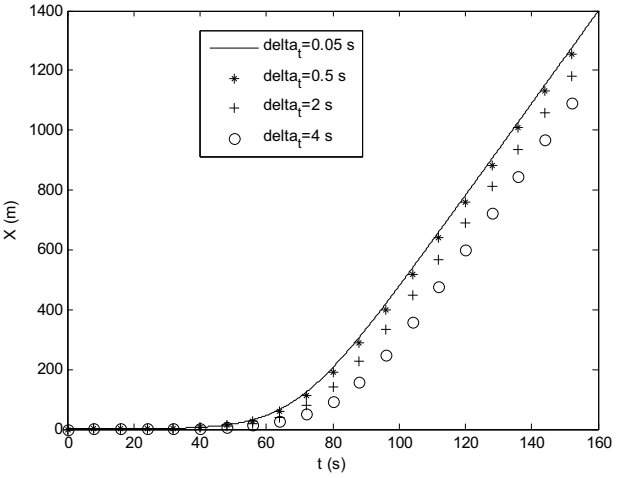

Figure 5. Underwater vehicle position along x-axis (global coordinate).

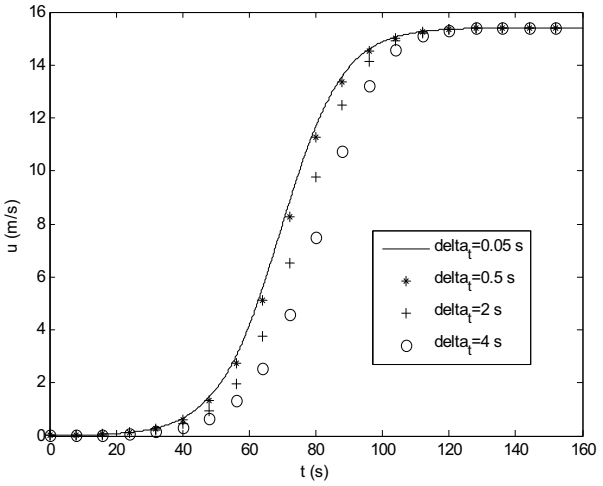

Figure 6. Underwater vehicle velocity along x-axis.

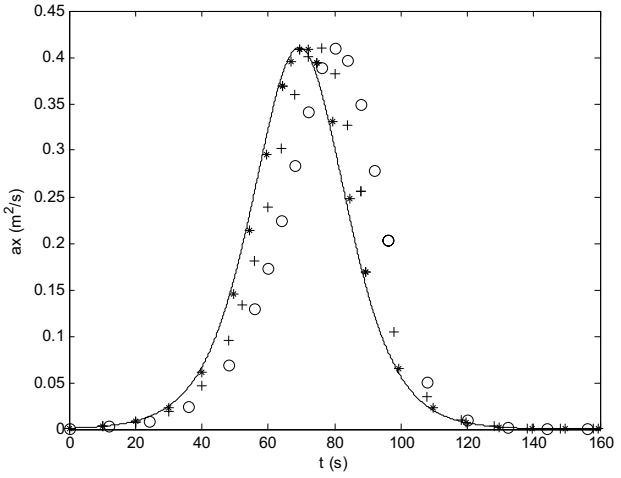

Figure 7. Underwater vehicle acceleration along x-axis.

Even with the very large time step of 4 seconds the modeling trends look reasonable, but there is an offset in the position, velocity, and acceleration curves. The propeller is working with the constant speed of 150 rpm, thus the vehicle with an initial surge speed of 0.01 m/s starts to move and accelerates under the thrust force up to a constant speed of 15.32 m/s. With the large time step the acceleration resulting from equation (23) peaks behind the values found using a smaller time step, though the magnitude is the same. All of the figures 5 to 7 show a delay in the simulation peaks for large time steps. Several other simulations with different time steps for different maneuvering situations showed similar results and indicated the convergence and stability of the code.

(b) Simulation Validation

The free-running model turning tests of the U.S. Coast Guard 47 feet motor lifeboat reported by Lewandowski [1995] was used to check the validity of the numerical simulation. This was done, as data for an

underwater vehicle was not available at the time the validation was done. The results are expected to be comparable only for small speeds where wavemaking is negligible. In order to make use of the stock propellers of diameter 0.079 m (0.258 ft) the model of the lifeboat was to a scale of 1/9.032. The data were acquired for the model, but the turning trajectories in the report are presented for the full-scale, after being measured from overhead photographs [Lewandowski 1995]. The principal dimensions of the prototype lifeboat and our underwater vehicle are given in Table 3(a) and (b). The underwater vehicle for the validation simulation had dimensions of approximately the same magnitude as the lifeboat. Its diameter was assumed to correspond with an average of the lifeboat's breadth and draft (the design draft was read from the body plan [Lewandowski 1995]). However, more important for the dynamics of maneuvering is to keep the submerged mass of the underwater vehicle consistent to the lifeboat's displacement, therefore the length and diameter of the underwater vehicle are slightly smaller than the lifeboat principal dimensions. The lifeboat has two propellers, but the underwater vehicle model has one propeller of a larger diameter.

A set of the lifeboat free-running tests, measuring its turn for two different approach speeds of 10 and 27 knots (5.15 and 13.92 m/s) with a 20-degree rudder angle was used to attempt to partially validate the underwater vehicle simulation. The rudder angle was reached at a high rotation rate of 10 deg/s. For the underwater vehicle simulation input is the propeller speed; the low and high approach speeds were modeled by different propeller speeds. The low rpm of 300 gives a steady state velocity of about 5.12 m/s, which after applying the 20 degree rudder angle reduces to about 5.02 m/s, and the high rpm of 815 gives a steady state velocity of about 13.91 m/s, which after applying the 20 degree rudder angle reduces to about 13.65 m/s. Figure 8 shows the results. Although the simulation can be done for any duration of time, the data were not presented for a complete turn to be consistent with the lifeboat data [Lewandowski 1995], which includes 31.3 and 18.6 seconds of data for the low and high approach speeds respectively. As can be seen, the simulation trends and magnitude are qualitatively consistent with the lifeboat tests although they do not agree quantitatively. Similarly to the lifeboat, the underwater vehicle at high speed first goes further but then has a sharper turn and intersects the low speed curve (the lifeboat has the same pattern of sharp turn for high speed but the data is not recorded long enough to show the intersection). Moreover, the simulation times are comparable that is, 32 s (dotted line) and 13.5 s (solid line) for low and high speed. Obviously, the hydrodynamics of the two cases are very different: the former is in deep calm water and the latter is on the surface with wave-making, water spraying, and other effects.

Length between perpendiculars (m)	13.080
Max. beam at chine (m)	4.270
LCG (m)	7.9
Displacement (kg)	19061
Propeller diameter (m)	0.71

(a)

l	10
d	2
x_B	4.16
m	21912
d_p	0.9

(b)

Table 3. Particulars of (a) the 47 ft motor lifeboat 1/9.032 model and (b) underwater vehicle.

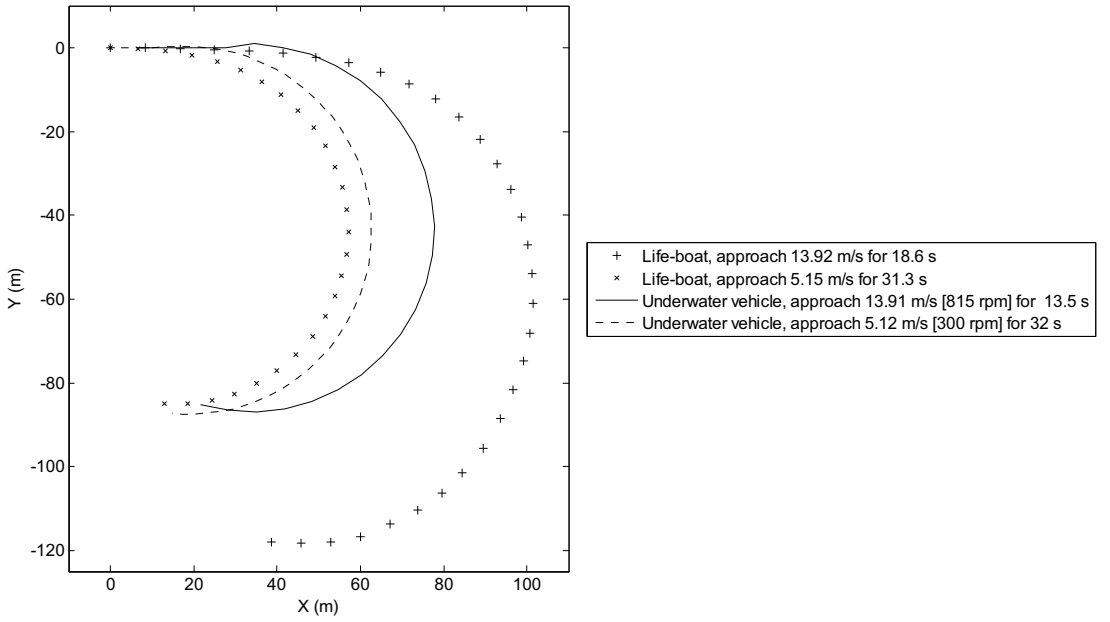

Figure 8. Effect of approach speed on turning trajectory; rudder: 20 deg; underwater vehicle simulation compared to the free-running lifeboat test data.

(c) Turning Maneuvers

This study considered a large submarine of length-to-diameter ratio 70m/12m with characteristics as shown in Tables 1 and 2, but the upper and lower rudders took an angle of 15º relative to the hull so that the underwater vehicle turned in the x-y plane. A diagram of position in the x direction for 600 seconds is shown in Figure 9. Figure 10 demonstrates the underwater vehicle turn in the horizontal plane. As seen in Figure 9, the underwater vehicle completes more than three turns and zooming-into Figure 10 the radius of the turn is found to be a constant value of about 368 m after the second turn. Moreover, comparing the surge velocities of this turn (not shown) with the ones in Figure 6, the steady state speed is less in the turning maneuver. The difference is about 0.5 m/s.

Note that this turn is different from the validation turn shown in Figure 8 section 4(b); for validation runs a straight course period of simulation was added in order to attain the constant approach speed before the rudders were set to the 20-degree angle. But, in this section the vehicle starts from a stationary state with an inclined rudder and a constant propeller speed of 150 rpm. To see the difference, Figure 11 shows both types of turns: the solid line is the turn from a stationary state with initially 15º inclined rudders (same as figure 10 but for shorter time), and the dashed line is a turn with an approach speed of 15.32 m/s, that is, the straight-course motion of section 4(a) for 160 seconds and then at zero x and y coordinates a high rate is applied to the rudder angle up to 15º. The result is significantly different from that of the rudders inclined from a stationary state: starting from a stationary state, it takes longer for the vehicle to initiate the turn and within the same duration of time the vehicle completes about one turn, while when the rudder angle is applied to

the moving submarine, the vehicle turns about 1.75 cycles in the same time. The radius of the turns is about the same. The focus here is on the initially stationary case, because the turn with a non-zero approach speed is actually a combination of linear surge motion and the turning side force of the rudders; however, here, the analysis of the turn itself with simple initial conditions was desired to illustrate the capabilities of the simulation code and to obtain some results for the turning maneuvers.

Going back to the 600-second simulation of the initially stationary vehicle with 15-degree inclined rudders, according to equation (15) (figure 12) the AOA of rudders relative to the water, a_r is changing with time, since β' is time dependent. Figure 12 shows the variation of the rudders' AOA versus time. Within about 200 seconds the surge, sway and yaw velocities, and therefore β' in equation (16), reach a constant value, and a_r reaches a constant value of 5.1º.

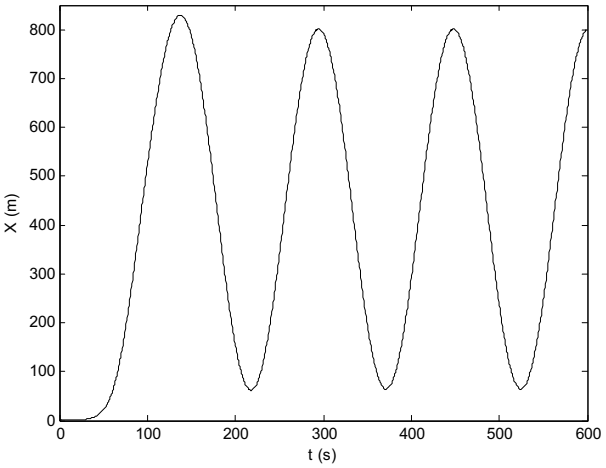

Figure 9. Underwater vehicle position along x-axis.

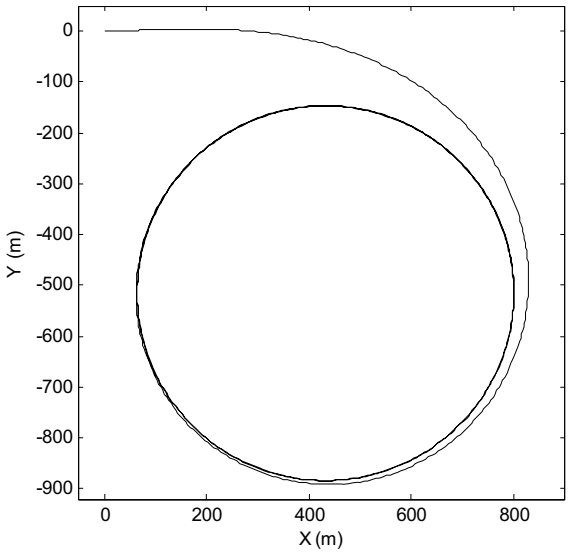

Figure 10. Underwater vehicle turn in x-y plane; rudder: 15 deg.

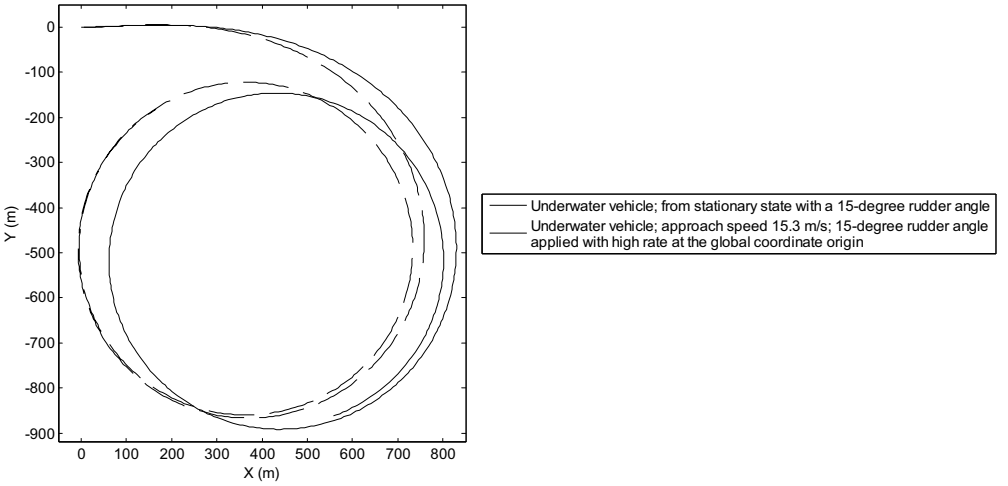

Figure 11. Turning maneuver simulation with rudders inclined from stationary state or at an approach speed of 15.3 m/s.

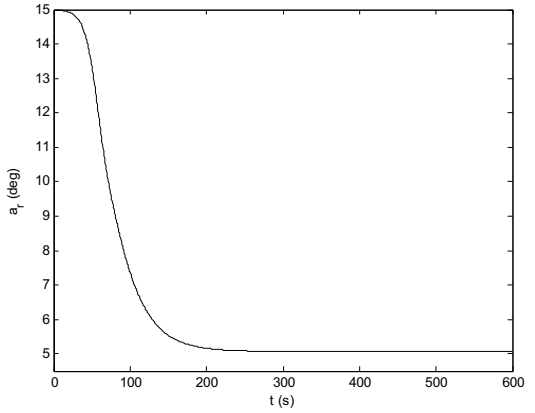

Figure 12. The change of AOA of the rudders.

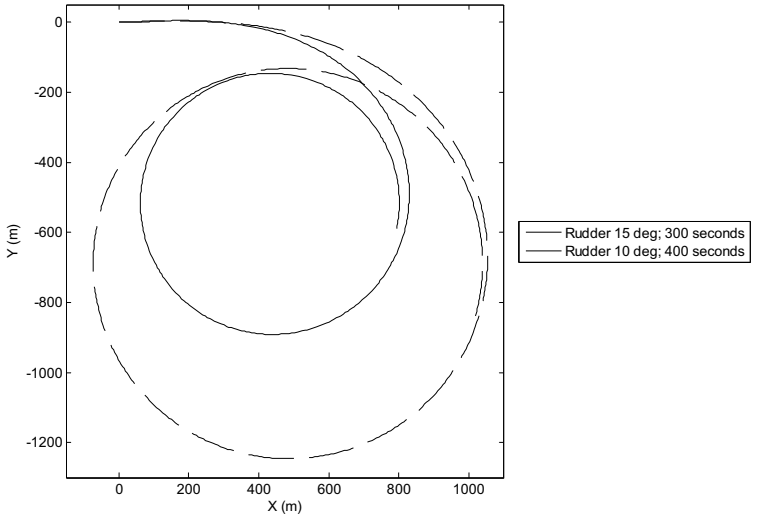

Figure 13. Turning maneuver with rudder angles 15 degrees and 10 degrees.

The same turning maneuver can be simulated for different initial rudder angles, a_{r0}. Figure 13 shows the turns with rudder angles of 15 degrees and 10 degrees with solid and dashed lines respectively. Both turns are about one cycle but with the larger rudder angle the turn takes less time. The turn with a smaller rudder angle has a greater radius and a slower rate of turn.

For the same vehicle, Figure 14 shows the radius of turn of the vehicle versus the initial rudder angle. The radius is expected to decrease but the rate of decrease slows down as a_{r0} gets larger, i.e., for large angles the lift force does not go to infinitely large values and therefore the radius of turn does not tend to zero.

Another observation is that the ratio of steady-to-initial AOA, after the motion comes to a constant speed (constant radius of turn), has a constant value of around 0.34 regardless of the initial AOA, a_{r0}. E.g. see this ratio in figure 12, that is, $a_{rs} / a_{r0} \approx 5.1/15$.

The effect of the length-to-diameter ratio on the turning radius and the steady state rudder AOA, a_{rs}, were studied. For all the simulations the initial ruder angle for both rudders is 10º. The vehicle was assumed to have a constant diameter, $d = 12$ m, and a variable length from 48 to 240 m so that the ratio l / d varies from four to twenty, which in practice is a very large range. The fore body of the vehicle was always one-fifth of the overall length, and the tip of the rudders was always $0.92 \times l$ away from the vehicle's fore end. Therefore both the distance of the center of buoyancy from the fore end, x_B, and the moment arm of the rudders, x_r, are increasing by the increase of length of the vehicle. The propeller was 5.4 m in diameter and constant rotational speed of 150 rpm. The turns were simulated and the steady state radius of turn and steady state rudder AOA was recorded.

The radius of turn increased with an increase in l / d and the time of simulation to come to a stable turn is increases for larger l / d. It is possible to non-dimensionalize the radius of turn. If divided by *d*, which is constant, the data are only scaled, but if divided by *l* the resulting non-dimensional value might be more useful than the dimensional radius of turn. Figure 15 shows the variation of dimensional radius of turn, *Radius*, versus l / d.

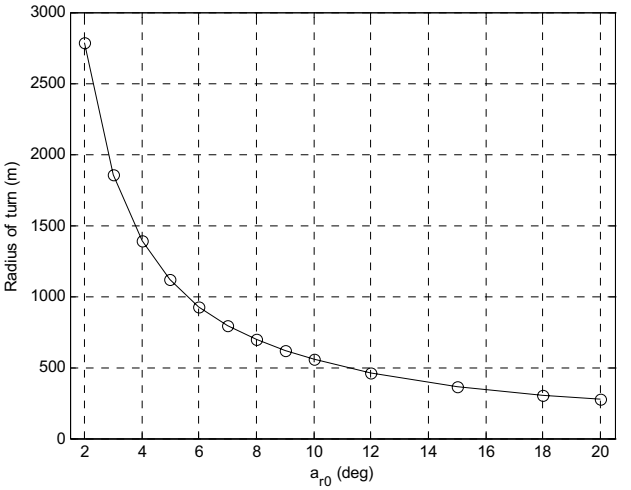

Figure 14. Turning radius vs. initial rudder AOA for $l / d = 70/12$.

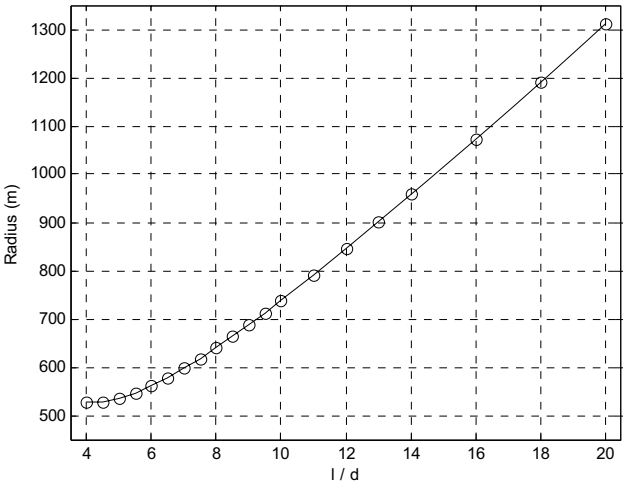

Figure 15. Steady state radius of turns vs. l/d for constant $a_{r0} = 10^{o}$.

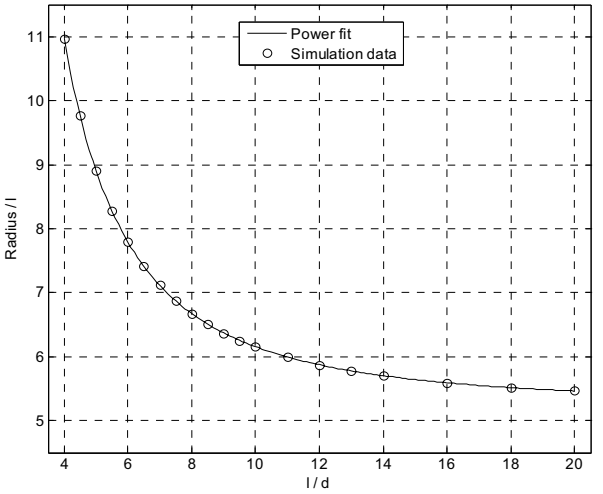

Figure 16. Steady state radius of turns: length ratio vs. l/d for constant $a_{r0} = 10^{o}$.

Figure 16 shows the variation of the dimensionless ratio: radius of turn: vehicle length, $Radius/l$, versus l/d. A power curve fitted to the data in figure 16, is as

$$(Radius/l)_{(a_{r0}=10^{\circ})} = 90.72 * (l/d)^{-1.99} + 5.23 \quad (24)$$

According to the fitted equation, which matches the simulation data, the ratio: steady radius of turn: vehicle length tends to a value of 5.23 as the ratio l/d tends to infinity.

The steady state AOA of the rudders, a_{rs}, was also non-dimensionalized dividing it by the initial angle of attack, a_{r0}. Figure 17 shows the variation of a_{rs}/a_{r0} versus the ratio l/d. The steady state rudder angle decreased with l/d increase, that is, after the motion comes to a steady state the rudders on the longer vehicle act with smaller AOA and that is one reason why the longer vehicle has larger turning radius. As the ratio l/d goes infinitely large, the ratio steady:initial AOA in figure 16 apparently

tends to zero, however it actually tends to a constant value slightly larger than zero and the vehicle turns very slowly. For instance, for $l/d = 200$ and initial rudder angle of 10º, the simulation resulted in a steady rudder angle of around 0.02º. Note that in Figure 17 the value for a_{rs}/a_{r0} for $l/d = 70/12 = 5.83$ is very close to the constant value of 0.34 mentioned previously for the value of $l/d = 70/12$.

(d) Propeller start up

In all the previous cases the propeller was assumed to have a constant rotational speed independent of time: 150-rpm. A more practical state of propeller start up can be simulated as well. The propeller was assumed to speed up at an exponential rate as in equation (27), i.e., the propeller starts from a stationary state and gradually, after a few minutes, attains a constant speed of e.g. 150 rpm in the form

$$n = 150 \times (1 - e^{-0.05t}) \qquad (27)$$

The diagram of acceleration along the x-axis is as in figure 18. Compared with the solid line in figure 7, it takes longer for the vehicle to accelerate. For these simulations, the average simulation time for 1000 seconds real time, with a time step of 0.1 s using a Pentium IV 3.00 GHz, is less than one minute.

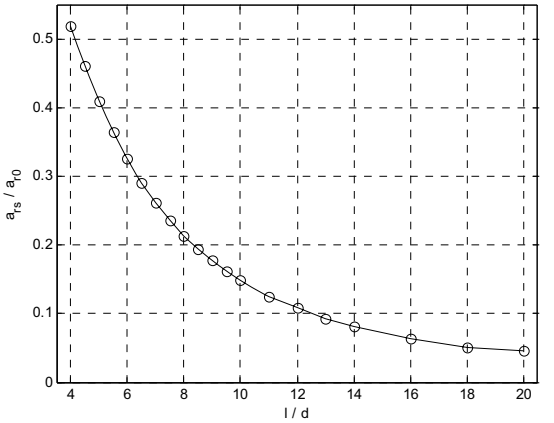

Figure 17. Variation in the steady state AOA of the rudders vs. the ratio l/d for $a_{r0} = 10º$.

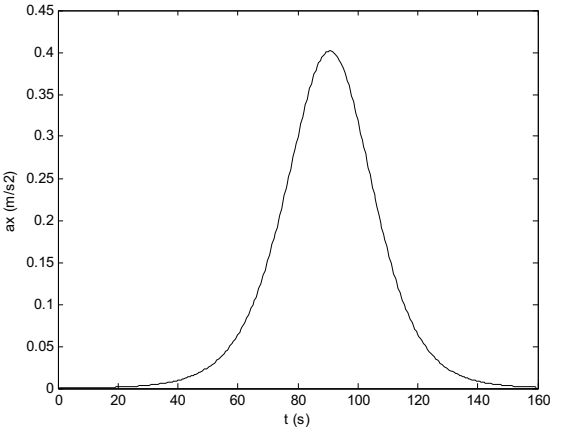

Figure 18. Underwater vehicle acceleration along the x-axis.

5. SUMMARY

The dynamics of an underwater vehicle including control fins and propeller was modeled and solved numerically. The small change of the model's response by a major change in time step revealed convergence in the numerical solution, and a turning maneuver simulation compared with free-running test data for a motor lifeboat (surface vessel) indicated the validation of the simulation.

Based on the simulations, the following conclusions were drawn:

- The radius of turn increased with length-to-diameter of the vehicle.
- Steady state angle of attack of the rudders decreased with length-to-diameter ratio.
- The difference of the turn trajectory for a vehicle with deflected rudders from stationary state and the one with a non-zero approach speed was observed to be significant.
- As the ratio l / d tends to infinity, the ratio: steady radius of turn: vehicle length tends to a value of 5.23, and the steady rudder angle of attack tends to a positive value slightly larger than zero.
- Propeller start up simulation showed that the real case of the gradually speeding up propeller needs a longer time to accelerate than the initially stationary vehicle.

ACKNOWLEDGMENTS

The authors warmly thank the Sharif University of Technology, Iran, and Memorial University, Canada for their support of this study. Many thanks to the editorial board of the previously published Ocean Engineering International and the present Journal of Ocean Technology for their corrections and contributions.

REFERENCES

1988 Society for Underwater Technology, submersible technology: adapting to change. 1988 In *Proc. of SUBTECH'87*, **14**, Graham-Trotman.

Allmendinger, E. E. 1990 *Underwater vehicle systems design, Written by a group of authorities.* The Society of Naval Architects and Marine Engineers.

Azarsina, F. 2004 *Underwater vehicle motion control.* Master Thesis, Sharif University of Technology, Tehran.

Azarsina, F. and Seif, M. S. 2005 *Principles of underwater vehicle dynamics modeling.* 1st International Conference on Modeling, Simulation and Applied Optimization, Sharjah, U.A.E.

Burcher, R. and Rydill, L. J. 1995 *Concepts in underwater vehicle design.* Cambridge University Press.

Carlton, J. S. 1994 *Marine propellers and propulsion.* Butterworth-Heinemann.

Fossen, T. I. 1994 *Guidance and control of ocean vehicles.* John Wiley & Sons Ltd.

Griffiths, G. 2003 *Technology and applications of autonomous underwater vehicles.* Taylor & Francis.

Humphreys, D. E. and Watkinson, K. W. 1978 *Prediction of acceleration hydrodynamic coefficients for underwater vehicles from geometric parameters.* Tech. Report # NCSL-TR -327-78, Naval Coastal Systems Laboratory, Panama City, FL.

Jackson, H. A. 1983 *Underwater vehicle parametrics.* International Symposium on Naval Underwater vehicles, RINA, London

Kuiper G. 1992 *The Wageningen propeller series.* MARIN Publication.

Loid, H. P. and Bystrom, L. 1983 Hydrodynamic aspects of the design of the forward and after bodies of the submarine. International Symposium on Naval Submarines, RINA, London.

Ridley P. 2003 Underwater Vehicle Dynamic Modeling. Queensland University of Technology.